Phase diagram of $BiFeO_3$/$LaFeO_3$ superlattices: antiferroelectric-like state stability arising from strain effects and symmetry mismatch at heterointerfaces

*Benjamin Carcan, Houssny Bouyanfif**, *Mimoun El Marssi, Françoise Le Marrec, Loic Dupont, Carine. Davoisne, Jérôme Wolfman, Donna C. Arnold*

Dedicated to Prof. Y . Yuzuyk

B. Carcan, Dr. H. Bouyanfif, Prof. M. El Marssi, Dr. F. Le Marrec
LPMC EA2081, Université de Picardie Jules Verne, 33 Rue Saint Leu,
80039 Amiens, France
E-mail: houssny.bouyanfif@u-picardie.fr
Loic Dupont, Carine. Davoisne
LRCS UMR7314, Université de Picardie Jules Verne,
33 Rue Saint Leu, 80039 Amiens, France
Plateforme de microscopie électronique, Université de Picardie Jules Verne,
33 Rue Saint Leu, 80039 Amiens, France
Dr. J. Wolfman
[4]GREMAN UMR7347, Université de Tours François Rabelais, 20 Avenue Monge,
37200 Tours, France
Dr. D.C. Arnold
School of Physical Sciences, University of Kent, Canterbury, Kent, CT2 7NH, United Kingdom

Keywords: Multiferroics, superlattices, epitaxial strain, phase diagram

$(BiFeO_3)_{(1-x)\Lambda}/(LaFeO_3)_{x\Lambda}$ superlattices (SLs) have been grown using pulsed laser deposition and studied by x-ray diffraction, transmission electron microscopy (TEM) and Raman spectroscopy. The composition was varied, $0.30 \leq x \leq 0.85$, while the modulation period Λ was kept constant at about 10nm. Unit cell doubling signatures typical of orthorhombic Pnma symmetry for x= 0.80 and 0.85 SLs and ¼{011} antiferroelectric $PbZrO_3$ like reflections in SLs with $0.30 \leq x \leq 0.7$ are detected by TEM showing a complex structural mixture at the nanoscale level. The Raman spectra confirm these observations and show a change in the SLs from a Pnma $LaFeO_3$ like spectra for $LaFeO_3$-rich period to a $PbZrO_3$ like spectra for $BiFeO_3$-rich period. Electron-phonon interactions and resonant-like excitations were also observed in the SLs. A temperature dependent x-ray diffraction investigation shows a large shift of the paraelectric-antiferroelectric phase transition scaling with the $BiFeO_3$ thickness. This shift is correlated with the strain state and can be explained by a strong interplay between octahedral rotation/tilt and anti-polar Bi displacement. Thickness-temperature phase diagram is constructed and differs from previous report showing the extreme sensitivity of the $BiFeO_3$ phase stability to strain effects and rotation/tilt degrees of freedom.

1. Introduction

Bismuth ferrite ($BiFeO_3$ or BFO) is the most studied multiferroic due to its robust ferroelectric state (T_C = 1100K) coexisting at room temperature with an antiferromagnetic order (T_N=640K).[1] Such coexistence and the possible cross coupling between both ferroic orders paves the way to so-called MagnetoElectric RAM combining advantages of the ferroelectric and the antiferromagnetic state.[2] Due to its high spontaneous polarization BFO has also been considered as an alternative to lead based solid solutions for electromechanical applications. Applications in BFO thin film form and bulk are limited by the high leakage currents and chemical substitutions were used in order to improve the physical properties.[3,4] Rare earth substitution of Bismuth ($Bi_{1-x}RE_xFeO_3$) via the combinatorial thin film synthesis allowed the fast investigation of the complete phase diagram of different solid solutions (RE: Sm, Gd, Dy, La).[5,6] Important piezoelectric properties were observed for some compositions (Sm, Gd) and were correlated to a morphotropic phase boundary (MPB) between a rhombohedral R3c (n°161) phase (low concentration of RE) and an orthorhombic Pnma (n°62) phase (high concentration of RE).[6] For instance MPB is observed at x_c= 0.14 for Sm and x_c decreases as the RE ionic radii decreases. Moreover for a limited range above x_c=0.14 an electric field induced double loop hysteresis is observed. [6] Local ordering has also been detected using transmission electron microscopy (1/4{110} reflections) which closely resemble the antiferroelectric (AFE) $PbZrO_3$ state. [6-7] The macroscopic state for this range of compositions still shows ferroelectric response and the AFE state seems to be limited to local regions. Similar to Sm, Dy and Gd substitutions, La induces a complex crossover (MPB) from a R3c symmetry to a Pnma symmetry but this is however not accompanied with giant piezoelectric responses. [6] The equivalent ionic radius between La and Bi and the absence of chemical pressure explain such a difference.[5-7] Note that the Bi electron lone pair is an important ingredient for appearance of the ferroelectric distortion and substitution by La somehow provokes ferroelectric “dilution”. In analogy to lead based solid-solution such MPBs in $Bi_{1-x}RE_xFeO_3$ are believed to be a structural bridge between the R3c and the Pnma phases. The mechanism of polarisation rotation and adaptive phase are the two models put forward to explain the emergence of MPBs.[8] While polarization rotation might explain MPBs in Ferroelectric-Ferroelectric (FE-FE) solid solution this is not the case for FE-AFE solid-solution and the adaptive phase model with extreme shrinking of the domain sizes has been used to explain MBPs in $Bi_{1-x}RE_xFeO_3$.[8] A further development has been made after the discovery of an incommensurate structure by TEM investigations.[7] Flexoelectric interactions have been introduced to explain such modulated incommensurate structures and the decrease of domain wall energy (effective negative domain wall energy).[8] According to this model competing distortion and octahedral tilt ordering ($a^-a^-a^-$ vs $a^-a^-c^+$) are accommodated via a modulated incommensurate structure and electromechanical softening yields giant piezoelectric responses. Artificially manipulating antagonistic order would not only allow for a better understanding of their interactions but also the design of nanostructures with remarkable properties. This strategy has been implemented in superlattices of complex oxides such as superconductor/ferromagnetic, relaxor/ferroelectric and paraelectric/ferroelectric.[9-16] In particular polarization rotation has been observed along with a MPB in $PbTiO_3$/$CaTiO_3$ superlattices.[16] In this work we have artificially introduced competition between R3c and Pnma orders by growing $BiFeO_3$/$LaFeO_3$ (BFO/LFO) superlattices. BFO and LFO present pseudo cubic unit cell parameters of 3.96Å and 3.92Å respectively in bulk. Considering only interlayer elastic interaction we expect BFO (resp. LFO) layers to be under in-plane compressive (resp. tensile) strain. Rispens *et al.* have investigated BFO/LFO superlattices coherently grown on orthorhombic $DyScO_3(110)_O$ substrates and revealed a complex structural behaviour that strongly depends on the composition and temperature.[17] Unfortunately the exact symmetry is not revealed for the region of the phase diagram at the boundary between the R3c Rhombohedral phase and the Pnma orthorhombic phase.[17] Maran *et al.* have also investigated superlattices with similar materials and found depending on the composition signs of an antiferroelectric-like state, incommensurate structures and the interesting possibility to tune the dielectric properties.[18,19] The superlattices they have studied are based on pure BFO layers combined with layers of a $(Bi,Sm)FeO_3$ solid solution made by combinatorial deposition and it is difficult to disentangle the effects of the alloying from the superlattice ordering.[18,19] We focus here on two sets of superlattices grown on cubic $SrTiO_3$(100) and MgO(100) substrates of about 8-9nm periodicities and complement the investigations by using Raman spectroscopy and TEM investigations (see supporting information) that are of importance for the evolution of the lattice dynamics (phonons linked to polarization and rotation/tilt ordering) and the detection of local ordering (AFE nano domains, incommensurate structure and unit cell doubling). Structural competition at the interfaces is probed via the synthesis of superlattices with varying ratio of BFO and LFO in the period ($(BiFeO_3)_{(1-x)\Lambda}/(LaFeO_3)_{x\Lambda}$ with Λ=8-9nm kept fixed and x varying from 0.25 to 0.8 with a total of 25 bilayers). For instance the superlattice $BFO_{0.5\Lambda}/LFO_{0.5\Lambda}$ shows the same ratio of BFO and LFO in the period (same thickness of about 4-4.5nm half the Λ wavelength/periodicity ; similar notation/terminology were used in references 10-15). The architectures of the two sets of SLs are given in the supporting information.

2. Results and discussions

2.1. Room temperature X-ray diffraction characterization

The superlattices have been characterized by in-situ reflection high energy electron diffraction (RHEED) and the streaks obtained on the diffraction patterns of all the superlattices indicate a smooth surface (see supporting information). **Figure 1** displays room-temperature θ-2θ x-ray diffraction pattern of the two sets of superlattices $BFO_{(1-x)\Lambda}/LFO_{x\Lambda}$ for $0.25 \leq x \leq 0.85$ grown on MgO and STO substrates. The MgO (respect. STO) substrates are buffered with a 20nm thick STO layer (respect. 40nm thick conducting $La_{0.5}Sr_{0.5}CoO_3$ layer). The MgO substrates give the possibility to investigate the SLs by Raman spectroscopy while the conducting $La_{0.5}Sr_{0.5}CoO_3$ (LSCO) buffer will enable electrical characterization. BFO and LFO single layers are also shown for comparison. No parasitic phases are detected within the limits of our instruments and all SLs and single films exhibit epitaxial growth. Satellite peaks indicate a modulated structure along the growth direction. Such satellite peaks are direct proof of a good crystalline quality and the synthesis of a modulated chemical structure and not a solid solution. The evolution of the satellite peaks positions and intensities reflects the change in the composition of the SLs from the LFO-rich period to the BFO-rich period. Rocking curves performed on the main satellite peak show a good crystalline orientation of all SLs.

Full width at half maximum (FWHM) of about 0.4° (resp. 0.1°) were measured for the SLs compared to 0.05° for the MgO substrate (resp. 0.01° for the STO substrate).

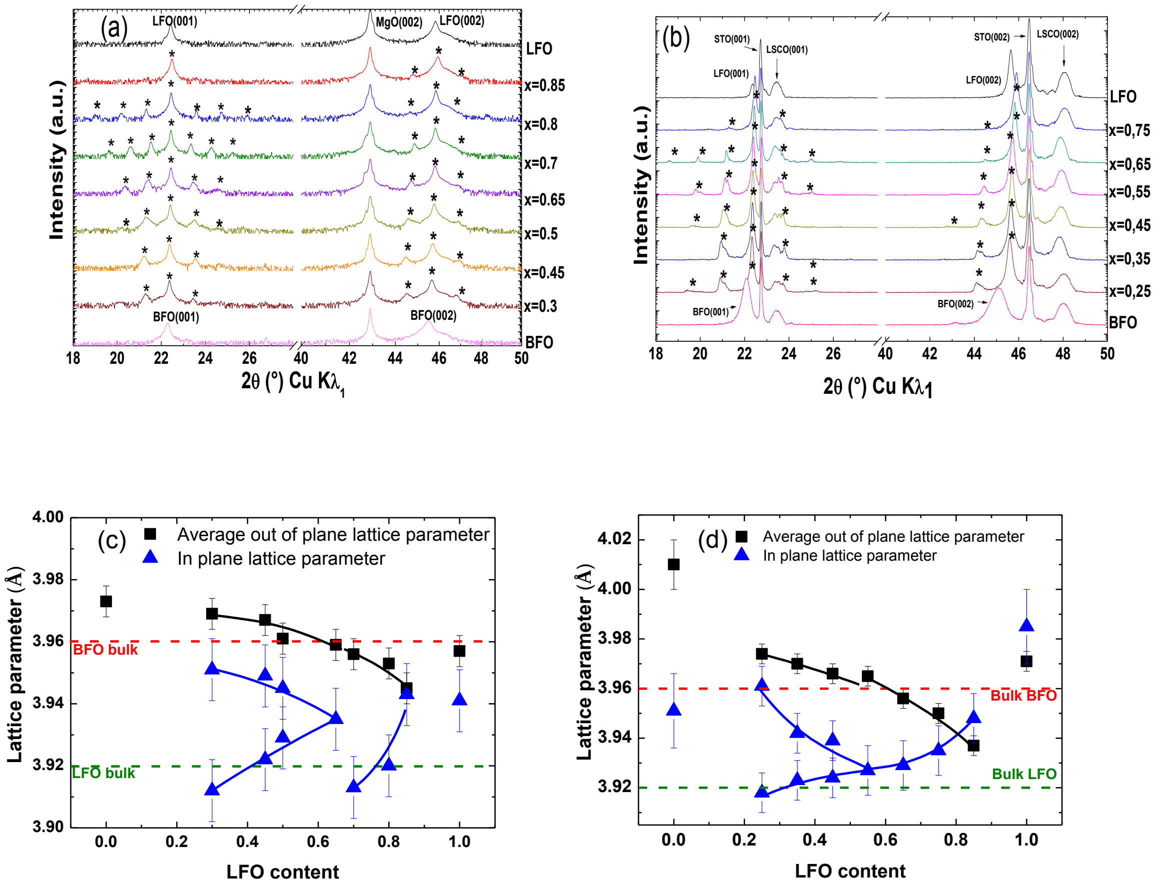

Figure 1. θ/2θ XRD patterns of $(BFO)_{(1-x)\Lambda}/(LFO)_{x\Lambda}$ superlattices as a function of x ($0 \leq x \leq 1$) grown on (a) MgO and (b) STO substrates (Asterisks denote the satellite peaks). Lattice parameters calculated for SLs deposited on MgO and STO substrates are respectively shown on (c) and (d). Pseudo-cubic bulk values are provided for comparison (dashed horizontal lines). Guide to the eyes are only shown for SLs.

Using the Bragg formula for SLs we have calculated an average out-of-plane lattice parameter for each superlattice from the 2θ value of the most intense satellite peak.[9-15] These results are presented in **Figure 1** and show a linear decrease of the average out-of-plane lattice parameter with increasing x. Such gradual behaviour has also been observed for out-of-plane lattice parameter of $Bi_{1-x}La_xFeO_3$ single films.[5,6] This decrease has been interpreted as a progressive diminution of the ferroelectric distortion when Bi is substituted by La. Note that while the Pnma state is reached above x_c=0.14 in clamped $Bi_{1-x}La_xFeO_3$ thin films, bulk investigations indicate a critical concentration of x_c=0.5.[20] The average out of plane lattice parameters do not perfectly interpolate with the thin film out-of-plane lattice parameter indicating a different global strain state in the SLs (particularly the case for the SLs on STO substrate). A direct comparison of the SLs with strain effects in thin films is not straightforward and interlayer interactions clearly need to be taken into account.

Reciprocal space mappings (RSMs) have been performed in order to explore the in-plane structure and to reveal the domain structures. Considering the multiple symmetries that BFO can adopt under strain we probed the (204) and (113) family of planes. Both RSMs show an important relaxation of the epitaxial strain between the multilayers and the cubic MgO and STO substrates. The different behaviour of the in plane lattice parameters detected on MgO and STO substrates indicates that residual strain is nevertheless present. As demonstrated below the residual strain seems not strong enough and similar structures are observed in both sets of superlattices. Such results suggest that interlayer interactions and symmetry compatibility between BFO and LFO in the SLs are the main driving force for any possible structural evolution with the ratio x of LFO. The STO buffer layer for the set of SLs grown on MgO substrates is not observed probably due to the low thickness (20nm) and weak diffraction intensity. For the set of SLs grown on STO substrates, the 40nm LSCO bottom electrode is coherently strained for all the SLs deposited on STO (see supporting information). Only one reflection has been detected for the (113) RSM excluding rhombohedral or monoclinic distortions (not shown) for all SLs deposited on MgO and STO substrates. However the (204) RSM shows a peculiar behaviour with a splitting detected for low values of x while only a single node is revealed for high values of x. This observation has been made for both sets of SLs deposited on MgO and STO. **Figure 2** shows the RSMs obtained for the x=0.3 and x=0.85 SLs grown on MgO and STO substrates. The RSMs measured for the (204), (024), (-204) and (0-24) family of planes are similar for all the SLs showing an in plane fourfold symmetry (see supporting information). A pseudo-tetragonal or orthorhombic average structure is therefore inferred from these measurements whatever the substrates. The SLs grown on MgO with x below 0.65 show a splitting (x below 0.55 for the SLs on STO). Such splitting is however not resolved at x=0.65 and above. A Large full width at half maximum (FWHM) for x above 0.7 is observed and is typical of Pnma LFO single layers (not shown). This is probably provoked by a domain structure with very small lateral correlation length (about 10nm for the x=0.85 SL on MgO for instance). Note that reflections are also observed at about Qz=10.2 (corresponding to a satellite peak) and around Qz=10.15. This last weak reflection appears at a Qz very close to the reflection observed for the x=0.8 SL and is probably of the same origin. Another domain orientation could also explain this reflection as discussed below (TEM investigation). The presence of such splitting and its evolution indicate a change of structure at about x=0.65-0.7 (resp. x=0.55) for the SLs deposited on MgO (resp. STO). As confirmed by TEM observations the structural coherency is maintained between the layers of the superlattices and the BFO and LFO layers present, within the limit of resolution of our diffractometer, the same in plane lattice parameters. The calculated in-plane lattice parameters are presented in **Figure 1** in comparison with the average out-of-plane lattice parameter and a complex structural behaviour is observed. The in-plane lattice parameters differ from the MgO and STO lattice parameter due to the epitaxial strain relaxation (see supporting information for Qx cross section of (204) RSMs). The differences in the two in plane lattice parameters decreases on going from x=0.3 to x=0.5 and a merging is observed at a value of x=0.65 for the samples grown on MgO (around x=0.55-0.65 on STO substrates). **Figure 1** shows an abrupt change of the in plane lattice parameters at 0.65-0.7 (resp. 0.55-0.65 on STO). Above x=0.7 the in plane lattice parameter increases. A structural phase transition is therefore observed on the SLs on increasing the LFO content and the same behaviour is revealed on both cubic MgO and STO substrates.

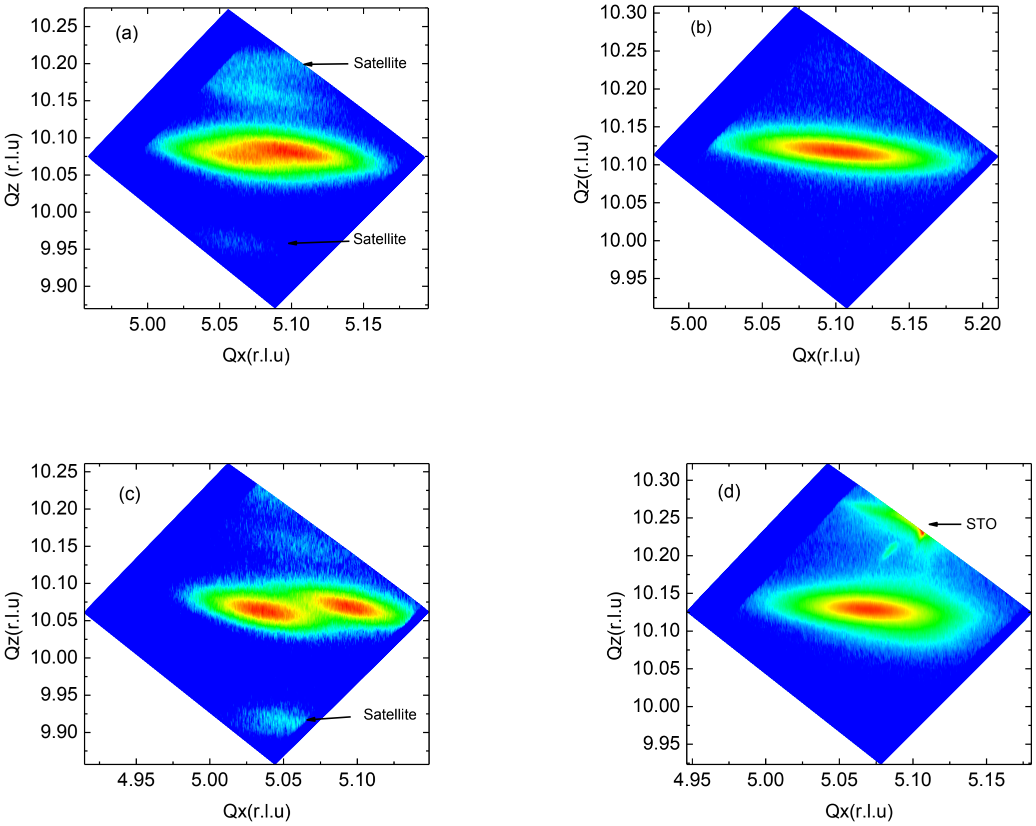

Figure 2. (204) Reciprocal space mapping of the SLs (a) $(BFO)_{0.7\Lambda}/(LFO)_{0.3\Lambda}$ and (b) $(BFO)_{0.2\Lambda}/(LFO)_{0.8\Lambda}$ grown on MgO.

(204) Reciprocal space mapping of the SLs (c) $(BFO)_{0.75\Lambda}/(LFO)_{0.25\Lambda}$ and (d) $(BFO)_{0.25\Lambda}/(LFO)_{0.75\Lambda}$ grown on STO.

A pseudo-tetragonal structure on average is deduced for the LFO thin film ((204) and (024) RSMs are similar) while the relaxed BFO thin film symmetry is R3c bulk like (RSM not shown). Such behaviour in the LFO thin film has already been observed (90° twinning, fourfold in plane symmetry and out-of-plane epitaxial strain) and a similar microstructure is described elsewhere.[21]

2.2. Transmission electron microscopy characterization

To better understand the XRD results and the effect of varying the ratio of BFO versus LFO on the microstructure of the superlattices we have undertaken transmission electron microscopy (TEM) studies. We discuss the results obtained on the set of samples deposited on MgO. Similar results were obtained on one SL deposited on STO (low ratio of LFO x=0.25; not shown below). Cross section images measured by TEM (see supporting information for SLs with x=0.45, x=0.65 and x=0.8) reveal good quality interfaces between each layer in the superlattices and between the 20nm thick STO buffer and the MgO substrate. Linear defects are, however, detected and are attributed to threading dislocations running through the entire thickness of the structure. Periodic nucleation of dislocations due to the very large mismatch has also been detected at the STO/MgO interfaces and explains the epitaxial relaxation between the substrate and the different layers (see supporting information for the TEM investigation of the STO buffer layer). A zoomed in region of the x=0.45 superlattice reveals a peculiar nanoscale dense lamellar structure that are oriented perpendicular and at 45° relative to the interface (see **Figure 3**). Such dense lamellar structures have also been observed on the x=0.65 but are absent for the x=0.8 superlattice.

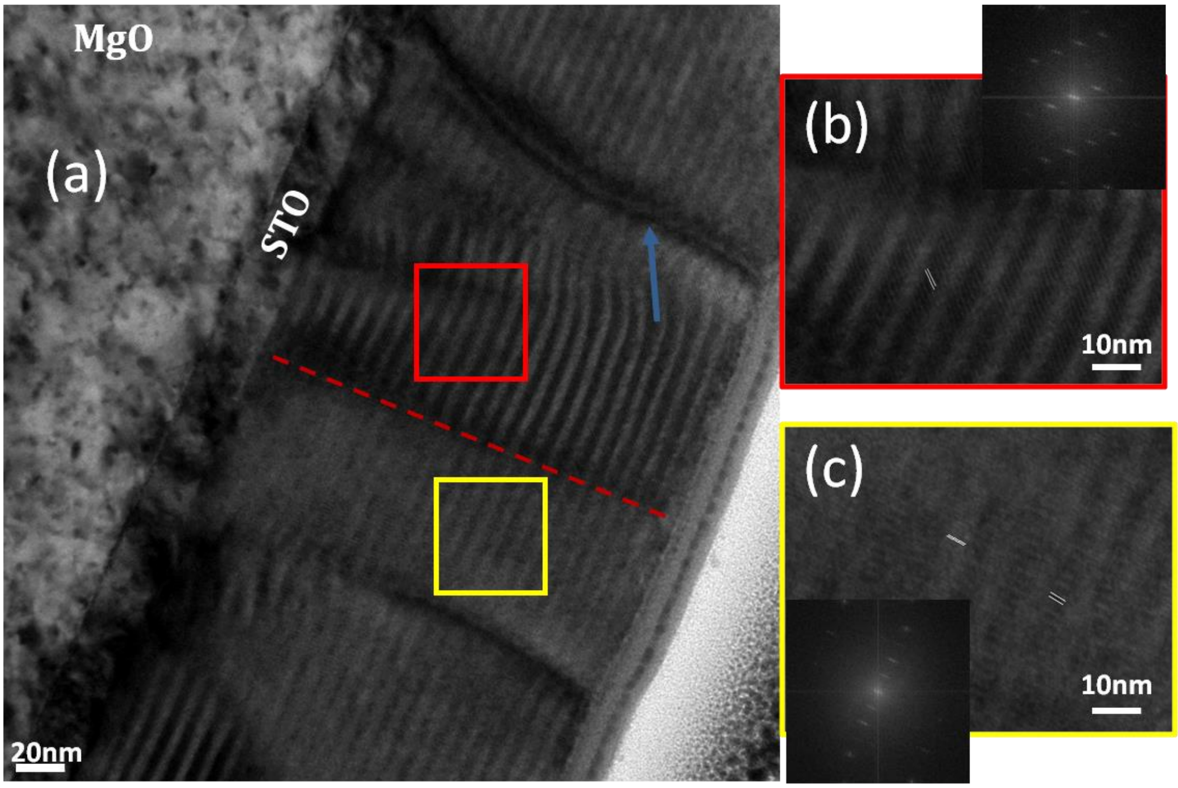

Figure 3. (a) Cross section image for the x=0.45 superlattice (scale bar at the bottom left : 20nm) (b) zoomed in region delimited in (a) by the red square highlighting the 45° oriented dense lamellae in the BFO layers (c) zoomed in region delimited in (a) by the yellow square highlighting the vertical dense structure in LFO and BFO. A vertical domain wall separates these two regions (dashed red line in (a)). The arrow indicates a vertical threading dislocation crossing the entire thickness of the multilayer. The insets of (b) and (c) show the Fast Fourier transform (FFT) for each domain.

Similar dense domains have also been observed at the MPB of (Bi,Sm)FeO_3 thin film solid-solution and have been correlated to a $PbZrO_3$-like structure.[7] These modulated structures are indeed observed in $PbZrO_3$ relaxed thin films.[22] Adjacent layers in such dense lamellar structures oriented at 45° have been shown to be of opposite polarization. For the periodic 45° modulated structure a period of the bilayers of about 1.15nm is estimated from the cross section image (**Figure 3 (b)**). These 45° nanoscale domains seem to appear only in the BFO layers. The period for the vertically dense lamellar modulated structure (**Figure 3 (c)**) differs in the LFO and BFO layers with values of 0.8nm and 1.5 nm respectively. Antiferroelectric $PbZrO_3$ like reflections are associated with these 45° lamellar structures as deduced from the comparison of the fourier transform of **Figure 3 (b)** and electron diffraction pattern presented in **Figure 4**. This last figure shows [100] zone-axis selected-area diffraction (ZADPs) obtained on three $(BFO)_{(1-x)\Lambda}/(LFO)_{x\Lambda}$ superlattices corresponding to x=0.45, 0.65 and 0.8.

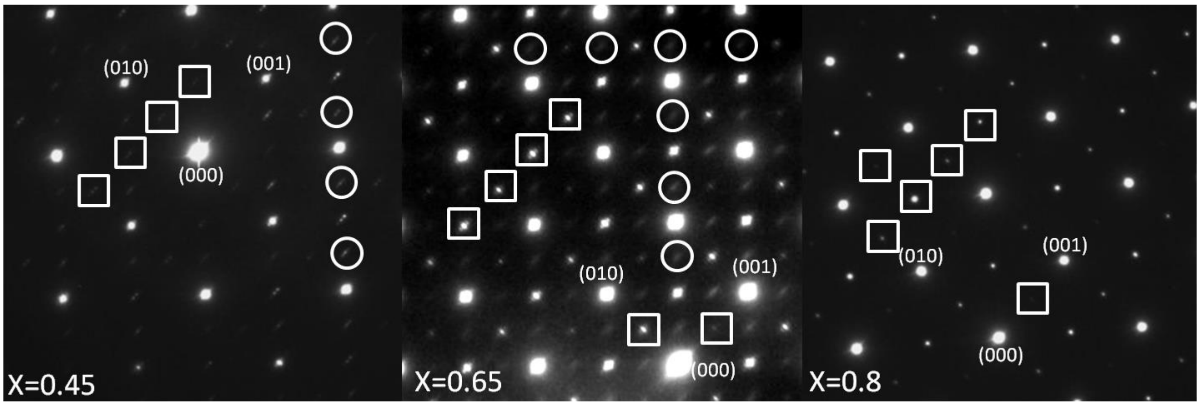

Figure 4. From left to right, [100]ZADP of $(BFO)_{(1-x)\Lambda}/(LFO)_{x\Lambda}$ superlattices with x=0.45, 0.65 and 0.8. Squares and circles indicate Pnma like reflections (1/2{001}, 1/2{010} and 1/2{011}) and $PbZrO_3$ like ¼{011} reflections respectively.

We observe satellite peaks oriented along the growth direction that are particularly clear for the x=0.45 and x=0.65 samples. Similar satellites have been observed by XRD and are direct proof of a chemical modulation along the growth direction. Inspection of the three diffraction patterns allows us to also detect the ¼{011} $PbZrO_3$ like reflections for x=0.45 and x=0.65 SLs (see circles). Such reflections indicate local anti-polar ordering similar to those observed in the $Bi_{1-x}La_xFeO_3$ MPBs. Note that the only SL deposited on STO with low ratio of LFO (x=0.25) studied by TEM also present $PbZrO_3$ like reflection. The lattice parameter derived from ¼{011} reflections is about 1.15nm coinciding with the period of the bilayers in the BFO lamellar structure (**Figure 3 (b)**). It is believed that this anti polar ordering mainly involves Bi-O atomic displacements. The reflections ¼{011} are no longer present for x=0.8 in agreement with the absence of the 45° lamellar structure. These reflections are directly connected with the 45° lamellar structure (see Fourier transform on **Figure 3 (b)**) and two orientations for such lamellar structures are observed for the x=0.65 SL. These two variants differ by the orientation of the in-plane c_o orthorhombic axis (along $[100]_{pc}$ or $[\bar{1}00]_{pc}$ and corresponding to the two different rows of circles on the x=0.65 diffraction pattern; see supporting information for a schematic representation of the orthorhombic unit cell orientation).[22,23] Furthermore the reflections 1/2{010} and 1/2{011} that are signature of unit cell doubling observed for the Pnma orthorhombic phase are also observed. The 1/2{010} Pnma like reflections are linked to the vertically oriented lamellar structure as deduced from the comparison with the Fourier transform (**Figure 3 (c)**). Although very weak, 1/2{001} reflection are also detected for x=0.8. The orthorhombic like unit cell dimension are found to be $a_{pc}\times a_{pc}\times 2a_{pc}$ in $Bi_{1-x}La_xFeO_3$ thin films where a_{pc} is the pseudo cubic unit cell lattice parameter explaining the 0.8nm period in the LFO layers estimated from **Figure 4 (c)**.[5,6] No ¼{0k0} reflections are detected while a $c_o=4a_{pc}$ is measured for some regions in the BFO layers (see **Figure 3 (c)**). Such reflections are extremely weak in bulk BFO MPBs and this could explain their absence on the diffraction pattern.[24] While both 1/2{010} and 1/2{011} reflections are intense for the x=0.65 superlattice they are extremely weak for x=0.45. It is obviously connected with the smaller ratio of LFO in the period for x=0.45. This result shows that Pnma like ordering is nevertheless quite robust and still present for such thin LFO layers (about 3nm for the x=0.45 superlattice). On increasing LFO ratio to x=0.8, the 1/2{011} reflection is stronger but the intensity of 1/2{010} reflections decreases. Similar observations have been made from TEM investigations of Sm substituted BFO thin film and might be explained by twin variants of the orthorhombic Pnma structure.[7] No $PbZrO_3$-like reflections are detected for the x=0.8 SL confirming the structural change suspected from the XRD results at x=0.65-0.7.

We believe therefore that the two kinds of domains presented in **Figure 3** (b) and (c) correspond to a $PbZrO_3$-like twin variant and a vertical domain wall separates these two variants (60° domain wall between domains with antiferroelectric axis along the $[0\bar{1}1]_{pc}$ and the $[\bar{1}01]_{pc}$ pseudo-cubic directions).[23,25] These two domains are responsible for the splitting observed on the RSM for x=0.3. The $PbZrO_3$ like unit cell dimensions discussed in the literature for RE doped BFO MPBs are $a_o=\sqrt{2}a_{pc}$, $b_o=2\sqrt{2}a_{pc}$ and $c_o=2a_{pc}$ (a_{pc}:peusdo-cubic unit cell parameter) for the Pbam group and $a_o=\sqrt{2}a_{pc}$, $b_o=2\sqrt{2}a_{pc}$ and $c_o=4a_{pc}$ for the Pnam type. Pbam and Pnam groups also differ in tilt system ($a^-a^-c^0$ for Pbam and a complex $a^-a^-c^+$/$a^-a^-c^-$ $NaNbO_3$ like for the Pnam system).[7,26] Pnma like LFO unit cell dimension are often described in thin film as $a_o=a_{pc}$, $b_o=a_{pc}$ and $c_o=2a_{pc}$ (different settings can be found in the literature but are equivalent to Pnma within a circular permutation of the coordinates). Considering the measured period for the BFO layers (1.15nm for the 45° bilayers periodicity and 1.5 nm on **Figure 3 (c)**) the unit cell seems to be described by the Pnam group with b_o=1.15nm ($\sim 2\sqrt{2}a_{pc}$) and c_o=1.5nm ($\sim 4a_{pc}$). For the domains with slabs tilted at 45° relative to the BFO/LFO interfaces (**Figure 3 (b)**) the unit cell orientation is such that $[100]_o$ //$[0\bar{1}1]_{pc}$, $[010]_o$ //$[011]_{pc}$ and $[001]_o$ //$[100]_{pc}$ (with the cubic system of reference given in the supporting information). The Bi anti polar atomic displacement (antiferroelectric axis) is along the $[100]_o$ //$[0\bar{1}1]_{pc}$ direction. Twin variants with the orthorhombic c_o axis along the four equivalent in plane directions are expected and explain the two type of domains observed in the cross sectional image and separated by a 60° domain walls. The pseudo-tetragonal structure detected by the reciprocal space mappings can be explained with this structural model. A pseudo-tetragonal unit cell is indeed often used for $PbZrO_3$ thin film considering the very small difference of lattice parameters along the $[\bar{2}10]_o$ and the $[1\bar{2}1]_o$ directions.[22,23] In this pseudo-tetragonal approximation the orthorhombic c-axis is parallel to the tetragonal c-axis. The splitting observed for x=0.3 is simply explained by the correspondance between the observed nodes with the different orientations of the $PbZrO_3$ like orthorhombic unit cell (or equivalently the pseudo-tetragonal unit cell with the c-axis lying in the plane). For the (204) RSM one diffraction node corresponds to domains with the orthorhombic c_o axis parallel to $[100]_{pc}$ (smaller in plane lattice parameter) while the second one is associated to domains with the orthorhombic c_o axis parallel to $[010]_{pc}$ (equivalent to the $[\bar{2}10]_o$ direction in the orthorhombic system of reference). On increasing x the $PbZrO_3$ like distorsion decreases. The associated splitting decreases and is no longer observed for high values of x (same behaviour for the superlattices deposited on $SrTiO_3$). The in-plane long axis of the LFO layers is aligned along the orthorhombic c-axis of the $PbZrO_3$ like unit cell of the BFO layers and the symmetry mismatch is therefore naturaly accommodated. As suggested by XRD and TEM we stress again that the structural coherency is maintained within the different layers of the SLs and it is not possible to assign different in-plane-lattice parameters to the BFO and LFO layers.

Observation of the ¼{011} $PbZrO_3$ like reflections in such SLs demonstrates the possibility of creating antiferroelectric order from a ferroelectric (BFO) combined with a paraelectric (LFO) in superlattices. The antiferroelectric order emerges only in BFO layers considering the strong tendency of the Bi to display polar ordering due to the electron lone pair.[27] Such antiferroelectric order cannot be explained by the nature of the epitaxial strain imposed on the BFO layers. Elastic interactions based on the difference of lattice parameters between LFO and BFO predict in plane compressive (resp. tensile) strain in BFO (resp. in LFO). Compressive strain does not solely explain the observed $PbZrO_3$ structure. Indeed for instance BFO adopts a monoclinic phase with a high tetragonal strain under a strong compressive strain (the so-called super-tetragonal phase). This is not what is observed in our SLs, so additional factors are necessary to explain the appearance of the $PbZrO_3$-like structure. Very recently considerations based on symmetry and octahedral tilt compatibilities at heterointerfaces have been used to better explain the structural behaviour of thin films and SLs based on complex oxides.[28] Therefore the driving force for the observed $PbZrO_3$-like structure is more likely to be the octahedral tilt compatibility at the heterointerfaces and the off-centric tendency of the Bi ion. Indeed the BFO layers of the SLs are shown to adopt the $a^-a^-c^+/a^-a^-c^-$ tilt system and the LFO layers the $a^-a^-c^+$ tilt (c here lying in the plane). We can not definitevely rule out Pbam $PbZrO_3$ symmetry and part of the sample may adopt the $a^-a^-c^0$ tilt system. The predicted orthorhombic $Pmc2_1$ in ultra short $BiFeO_3/LaFeO_3$ superlattices and BFO thin film is also a candidate since it is characterized by the coexistence of polar and antiferroelectric distorsion. [29,30] The observed $PbZrO_3$ structure is therefore not associated with alloying effects. Note that first principle theory predicts such complex tilt ordering and nanotwinned phases in BFO due to competing instabilities and the SLs have been shown to be an ideal platform for inducing new phases from interactions between different instabilities (antiferrodistortive versus ferroelectric ordering).[31,32] Connections are possible with the model proposed by Tagantsev *et al.* to explain the antiferroelectric ordering in $PbZrO_3$.[23] TEM refinement structure at the atomic scale would allow us to understand the interplay between polar displacement and octahedral tilt ordering at the heterointerfaces of the SLs. To gain a deeper understanding of the structure, these SLs have also been investigated by Raman spectroscopy.

2.3. Raman spectroscopy investigation

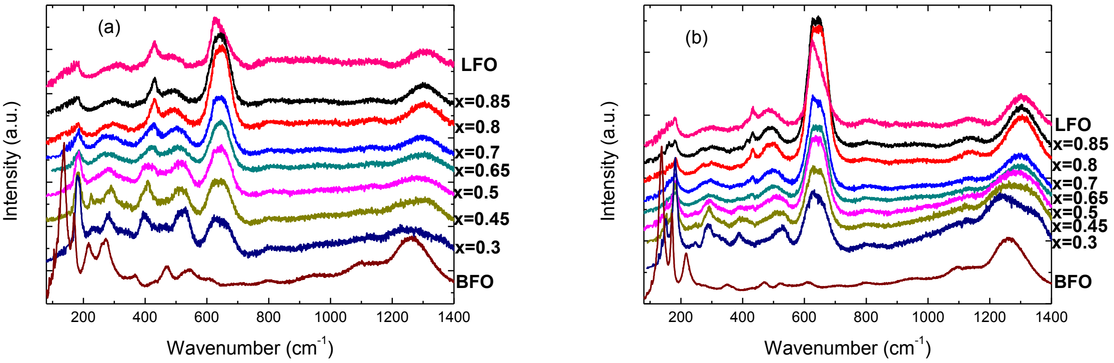

Figure 5. Room temperature Raman spectra of $(BFO)_{(1-x)\Lambda}/(LFO)_{x\Lambda}$ superlattices in (a) crossed ($Z(XY)\bar{Z}$)and (b) parallel geometry ($Z(YY)\bar{Z}$).

All SLs have been investigated by polarized Raman spectroscopy and **Figure 5** displays the room temperature Raman spectra recorded in crossed ($Z(XY)\bar{Z}$) and parallel ($Z(YY)\bar{Z}$) geometries. BFO (x=0) and LFO (x=1) single films are also shown for comparative purposes. These different geometries are useful to reveal the nature of phonon symmetries. For small values of x, two peaks below $200cm^{-1}$ are observed in the parallel geometry for the superlattices and are reminiscent of the BFO A_1 phonons.[33] These phonons appear at about $138cm^{-1}$ and $170cm^{-1}$ in the BFO film and a significant mode hardening is observed in the SLs. The doublet is observed at $150cm^{-1}$ and 181 cm^{-1} in the SLs suggesting a strong change in the Bi atomic displacement. Further comparison of the BFO film to the SLs indicates a change of relative intensity: the phonon at $181cm^{-1}$ being more intense in the SLs compared to the one at $150cm^{-1}$. The opposite is observed on the BFO film (mode at $138cm^{-1}$ more intense than the mode at $170cm^{-1}$). Changes of relative intensity of these two modes are often detected in ceramics due to the random orientation of grains but Raman spectra collected on different regions of the BFO thin film and SLs did not show any spatial dependence. These two phonons are characteristics of the R3c polar state in BFO bulk and thin films and provide a good spectral signature for any symmetry changes. This strong phonon hardening and the change of relative intensity are therefore probably connected to the change of polar ordering from ferroelectric to antiferroelectric $PbZrO_3$-like state in the BFO layers of the SLs as detected by TEM. The bands in the range $200cm^{-1}$-$300cm^{-1}$ involving oxygen octahedral tilt degrees of freedom present very different shapes for the $0.3 \leq x \leq 0.65$ compared to the BFO or LFO Raman spectra suggesting a different tilt ordering for these SLs. Note that the Raman spectra of the SLs ($0.3 \leq x \leq 0.65$) closely resemble the Raman spectra of the La doped BFO solid-solutions (x=0.2-0.5 $Bi_{1-x}La_xFeO_3$) studied by Bielecki *et al.*.[20] The authors argue that a $PbZrO_3$ AFE-like state is present for the x=0.2-0.5 $Bi_{1-x}La_xFeO_3$ composition. Note that the mode at 170cm^{-1} in bulk BFO overlap with the polar Bi ordering while the mode at 220cm^{-1} overlaps with the octahedral tilt degree of freedom.[33] Bielecki *et al.* use this last phonon to track the evolution of the tilt angle versus composition and the R3c versus Pnma phase stability.[20] This last phonon mode visible in the crossed polarization geometry (Figure 5 (a)) also shows a hardening in the SLs and is visible up to x=0.45 at a frequency of 226cm^{-1}. The Raman selection rules predict an important increase of Raman active phonon bands when going from the R3c to the $PbZrO_3$-like (Pbam, Pnam) symmetries that is unfortunately not possible in the Raman spectra collected for our SLs. As discussed by Goian *et al.* and Bielecki *et al.* in similar systems the discrepancy between the number of observed bands and the predicted number of active bands is explained by the very small distortion and therefore weak difference in frequencies or splitting between the different bands.[20,34] Strong damping and large bands also explain the impossibility to separate the different excitations and to identify the exact number of bands and phonon symmetries.

Similar Raman spectra and behaviour have also been observed for BFO under hydrostatic pressure. A change from rhombohedral like to orthorhombic like symmetries is inferred from X-ray diffraction and Raman spectroscopy under hydrostatic pressure and the Raman spectra at 4.1GPa is close to the one we observe for x below 0.65.[35] Such similarity is probably a signature of the orthorhombic symmetry and we mention in this context the theoretical investigation by Xue *et al.* on pressure induced Antiferroelectric like state in BFO based solid solution.[36] We must stress that care must be taken when comparing strain effects in thin films or multilayers with hydrostatic pressure investigations and magnitude of biaxial stress cannot be easily deduced from such comparison. Nevertheless Raman fingerprints of competing phases were detected by Guennou *et al.* and our Raman spectroscopy investigation combined with the TEM studies also indicate~~s~~ a complex nanoscale mixture.[35] Raman spectroscopy also revealed an electron-phonon and resonant like excitation in the superlattices at about 620 cm^{-1}. The progressive change from a BFO like state to a LFO like state is also clear from this strong phonon mode. This excitation probably corresponds to a doublet and is absent in the BFO thin film Raman spectra. An asymmetric peak is, however, observed in LFO at the same frequency. The origin of this excitation is not clear and two explanations are proposed and connected to local disorder: a Fröhlich activated Raman forbidden longitudinal modes and a disorder activated spin wave.[20,37] This last interpretation has been done on the basis of a spin wave dispersion investigation and the energy measured at the zone boundary. The combination and overtone of this strong and resonant like first order phonon modes gives rise to the second order Raman spectra visible at about 1200-1300cm^{-1}. We also clearly see in this second order scattering a progressive change from a BFO-like to a LFO-like excitations, with LFO second order excitations lying at higher frequencies compared to BFO. A complex mixture of two-modes is observed at intermediate compositions.

2.4. Temperature dependent X-ray diffraction and phase diagram

To study the relative phase stability and structural phase transitions in the SLs we performed x-ray diffraction measurements at different temperatures in the range of 25-625°C. Lattice parameters versus temperature of the substrates were systematically calculated and the expected thermal dilatation were observed for all samples investigated (not shown). For the set of SLs deposited on STO the LSCO buffer layers do not show any structural anomalies on heating and only a linear thermal dilatation is detected.

Average out-of-plane lattice parameters from room temperature to high temperature are shown in **Figure 6** (a) and (b) for the SLs deposited on MgO and STO respectively. Whatever the substrates, SLs with low content of LFO show important anomalies at high temperatures in contrast to SLs with a high content of LFO for which a linear dilatation is detected. These structural anomalies are only observed for SLs for which an antiferroelectric like state has been detected at room temperature. Such structural anomalies are therefore interpreted as a phase transition from the antiferroelectric-like state to a paraelectric like state. Figure 6 (c) and (d) present the corrected average out-of-plane lattice parameter for SLs showing structural anomalies (0.3≤x≤0.7 for MgO and 0.25≤x≤0.55). This correction allows for the removal of the linear paraelectric contribution to the average lattice parameter and to better evidence the distortion due to the polar ordering below the critical temperature.[38]

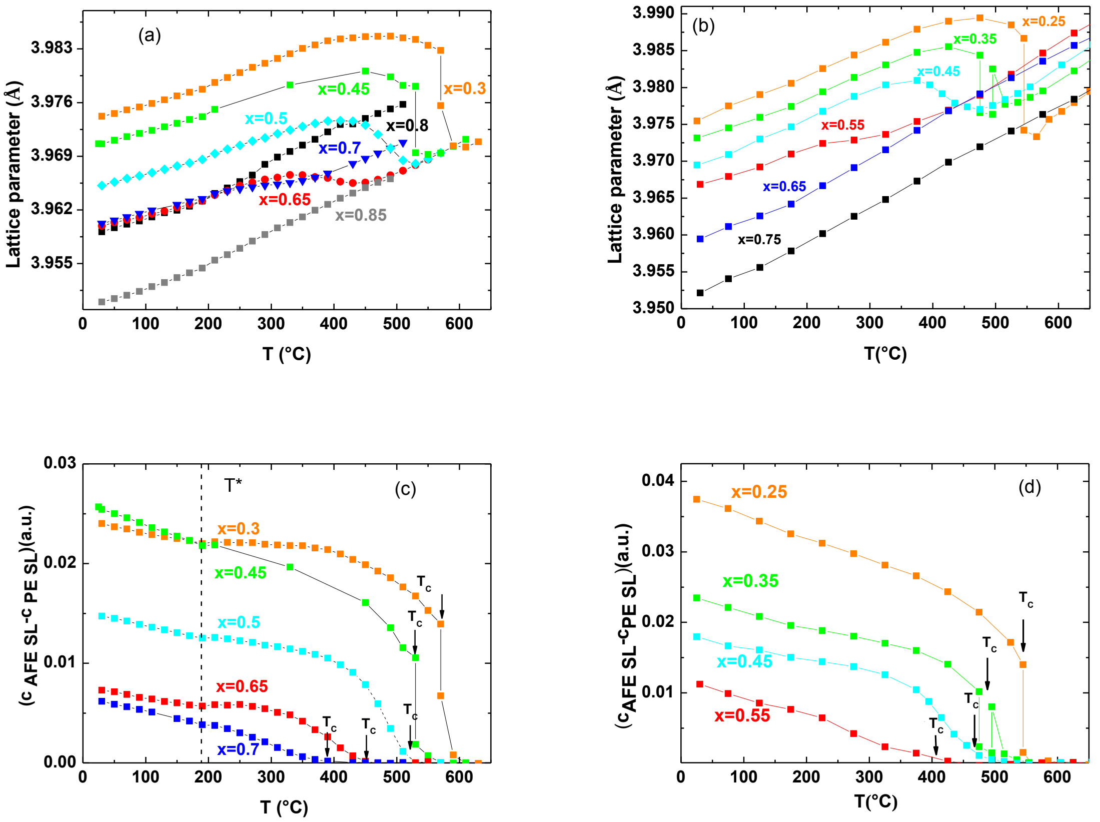

Figure 6. Average out-of-plane lattice parameter versus temperature for SLs deposited on (a) MgO and (b) STO. (c) and (d) show corrected average out-of-plane lattice parameter for SLs on MgO and STO respectively.

We clearly see a shift of the critical temperature (antiferroelectric to paraelectric) to lower temperatures when the ratio, x, of LFO increases. It is also equivalent to consider that Tc decreases when the BFO thickness decreases in the period for this set of samples. The SLs deposited on STO present a similar behavior. Rispens *et al.* also observed a scaling of the critical temperature with the BFO thickness in BFO/LFO SLs.[17] The octahedral tilt is believed to increase under strain and to efficiently relax the epitaxial strain in SLs. Complex interplay between strain, octahedral tilt and anti-polar Bi ordering probably explains the destabilization of the antiferroelectric state and the decrease of Tc. The role of flexoelectric interaction in these SLs needs also to be revealed in order to get a full understanding of the observed behavior of Tc. For x=0.3 the transition is abrupt typical of a first order phase transition. A splitting of the main satellite peak is observed and supports the first order nature of the transition. However when x increases the transition becomes more diffuse and no abrupt jump of the average out-of-plane lattice parameter is observed. For instance the x=0.65 and x=0.7 SLs behavior suggest a more diffuse phase transition. Superlattices with x=0.8 and 0.85 do not show any anomalies in the structural behavior suggesting a stability of the paraelectric phase at all temperature studied. These observations support our interpretation of Pnma-like symmetry for these SLs from the room temperature XRD, TEM and Raman investigations. This structural phase transition is understood as a $PbZrO_3$-like (Pbam, Pnam) to LFO-like (Pnma) transformation for low x. Finally an anomaly is observed at about 180°C (T*) that is independent of the BFO thickness and for both set of SLs deposited on MgO and STO substrates. Such T* independent of the strain have been detected in BFO thin films and bulk materials and seems to involve Fe-O bond length changes.[39-41] In bulk it has been attributed to surface transition (within a few nm) and proximity of the Neel temperature (267°C and 367°C for BFO and LFO respectively in bulk) may explain its origin. The anomalies observed at high temperature could be interpreted as a change of orientation or structural domains in the SLs and in order to rule out such possibilities we performed reciprocal space mapping at different temperatures. **Figure 7** presents the results obtained on the SL with x=0.35 on STO at selected temperatures. Figure 7 also shows the calculated in plane-lattice parameters from the Qx position. On increasing the temperature we observe on the RSM a decrease of the splitting in Qx. Such a decrease on heating suggests a decrease of the $PbZrO_3$-like orthorhombic distortion. At about 400°C the splitting is no longer resolved in Qx and only one broad node is observed. On further heating a splitting along Qz is detected corresponding to the structural phase transition. This behavior and the extracted in-plane lattice parameters confirm these interpretations of a structural phase transition from a $PbZrO_3$ like anti-polar phase to a high temperature paraelectric phase (Pnma). At the structural transition the low temperature and the high temperature phase coexist (splitting in Qz) which is a typical characteristic of a first-order transition.

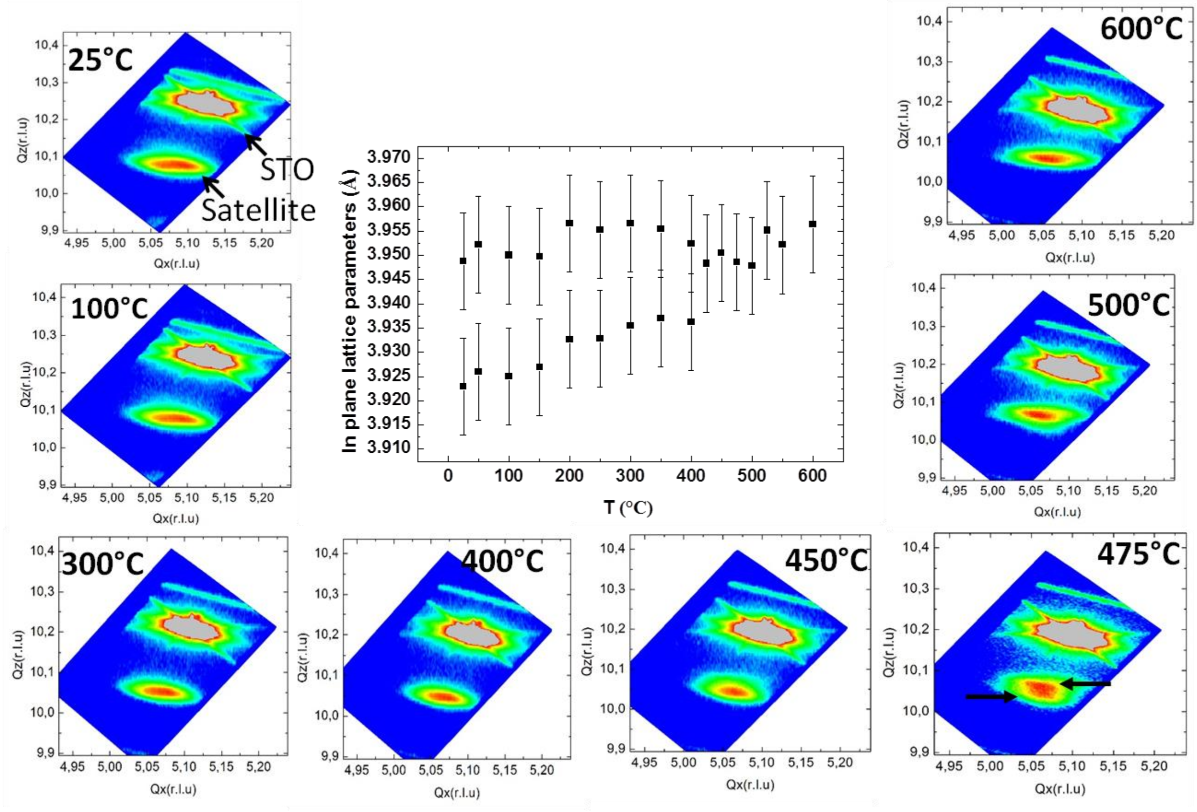

Figure 7. Reciprocal space mappings and in-plane lattice parameters as a function of temperatures for the $BFO_{0.65\Lambda}/LFO_{0.35\Lambda}$ SL grown on STO. A splitting in Qz is observed for a certain range of temperatures (see arrows at 475°C). An additional contribution from the sample holder is observed (ring like shape above the STO reflection).

SLs with fixed ratio of LFO (x=0.5) and different periodicities were also investigated and the results indicate that the main parameter controlling the phase stability is the BFO thickness of the layers in the SLs (results not shown). This behavior, in agreement with Rispens *et al.*, enabled us to construct a thickness-temperature phase diagram of the SLs (**Figure 8**).[17] Results obtained from Raman spectroscopy also rules out a structural phase transition down to 90K for the SLs deposited on MgO with a high ratio of LFO.

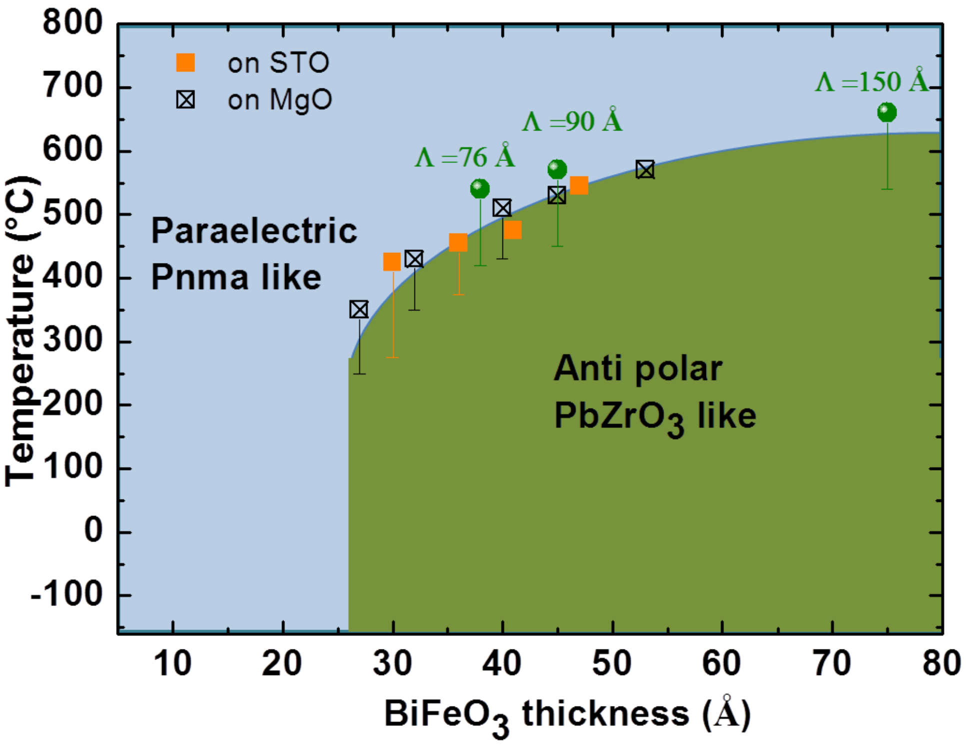

Figure 8. Phase diagram of BFO/LFO superlattices on (001) oriented MgO and STO substrates. Additional data (green spheres) obtained on $BFO_{0.5\Lambda}/LFO_{0.5\Lambda}$ SLs grown on MgO with three different Λ but fixed LFO content (x=0.5) are also plotted.

We note that the critical thickness at which the anti-polar state disappears for a fixed temperature is about 26Å very close to the value obtained by Rispens *et al.* for the disappearance of the ferroelectric-like state.[17] For increasing thicknesses above 75-80 Å we would also expect a transition to a Rhombohedral R3c-like state for the BFO layers of the SLs. The proposed phase diagram calls for a theoretical investigation to better understand the influence of thickness on the critical temperature, the anti-polar state stability and to identify the primary order parameter of such BFO/LFO superlattices. Preliminary results obtained on similar SLs deposited on $DyScO_3$(110) substrates do not, however, show $PbZrO_3$-like phases for BFO rich SLs. In contrast to the SLs deposited on MgO and STO a full structural coherency is observed on orthorhombic $DyScO_3$ (110) substrate (Pnma space group) and this probably explains the different phases observed by Raman and XRD. The structural imprint from the $DyScO_3$ substrate of the oxygen octahedral rotation/tilt system is also a key factor that must be taken into account to interpret the differences with the SLs deposited on cubic substrates. Since the anti-polar domain sizes (~1.15nm from TEM) do not scale with the BFO thickness we do not consider electrostatic effect as the primary driving force of this antiferroelectric order.[42] We are currently looking to investigate and understand the magnetic (magnetoelectric) behavior of such multiferroic SLs.

3. Conclusion

BFO/LFO superlattices have been grown and studied in order to better understand the structural interaction at the origin of the MPBs between the R3c rhombohedral state and the Pnma orthorhombic state. Such MPBs are believed to be due to competing distortion and octahedral tilt degrees of freedom. Our SL investigations reveal a nanoscale mixture that depends strongly on the BFO thickness ($PbZrO_3$ like versus Pnma like state). A $PbZrO_3$ antiferroelectric-like state in BFO and a peculiar domain state is revealed using a combination of XRD, TEM and Raman spectroscopy investigations. Octahedral tilt compatibility at the interfaces and off-centric Bi tendency probably explain the observed nanoscale modulated structure on the SLs deposited on cubic substrates. A temperature dependent x-ray diffraction study showed an important tuning of the antiferroelectric to paraelectric phase transition. Thermal stability of the antiferroelectric state is strongly sensitive to the strain and complex interplay between octahedral tilt and anti-polar Bi ordering may explain such behavior. A phase diagram is proposed and differs with previous reports on $DyScO_3$ substrates. The nature of the substrates (cubic versus orthorhombic) and structural imprint of the oxygen rotation/tilt system probably explain such differences. A variety of remarkable properties (piezoelectric and magnetoelectric) is expected for the MPB like state and is the subject of future investigations.

4. Experimental Section

BFO/LFO superlattices were grown on buffered (001) oriented MgO and $SrTiO_3$ substrates by pulsed laser deposition (MECA2000 chamber) using a KrF laser (248nm) at a 4Hz repetition rate. Both BFO and LFO were grown under 7.10^{-2} mbar of oxygen pressure (PO_2) at 775°C. For the set of SLs deposited on MgO a $SrTiO_3$ (STO) 20nm thick buffer layer was used to promote epitaxial growth and to favour the perovskite phase (it can be difficult to avoid parasitic phase in BFO layers directly grown on MgO). The important advantage of MgO and the reason for using it over other substrates is the possibility to investigate the multilayers by Raman spectroscopy since it is Raman inactive. The buffer layer of STO was deposited at 10^{-5} mbar of PO_2 and 800°C. For the superlattices grown on STO substrates a 40nm $La_{0.5}Sr_{0.5}CoO_3$ (LSCO) bottom electrode was used for future electrical measurements. Structural characterizations of the multilayers were performed using a high-resolution 4-circles diffractometer with a Cu $K\lambda_1$ parallel beam (Bruker Discover D8). Transmission electron microscopy (TEM) was performed using an S-TWIN FEI TECNAI F20 microscope on cross sections of samples prepared using a focused ion beam (FIB) technique. Prior to the FIB process a protecting platinum layer was deposited on the sample to avoid damages and amorphization of the SLs. Raman measurements were performed using the 514.5 nm line from an argon ion laser and analyzed using a Jobin Yvon T64000 spectrometer equipped with a charge coupled device. An optical microscope was used to focus the incident light as a spot of about 0.9 μm in diameter on the sample (objective x100). Scattered light was collected using the same objective of the microscope (back-scattering geometry). Using the Porto notation, Raman spectra were measured in crossed ($Z(XY)\bar{Z}$) and parallel geometry ($Z(YY\bar{Z}$). X, Y and Z corresponding respectively to [100], [010] and [001] of MgO crystallographic axes.

Supporting Information

Supporting Information is available from the Wiley Online Library or from the author.

Acknowledgements

H.B is grateful to Pr. I. Lukyanchuk for enlightening discussions on the electrostatic effects in ferroelectric superlattices. Financial support by the Picardy Region is gratefully acknowledged (project ZOOM).

References

[1] G. Catalan, J.F. Scott, *Adv. Mater.* **2009**, *21(24)*, 2463–2485.

[2] M. Bibes, A. Barthélémy, *Nat. Mater.* **2008**, *7*, 425.

[3] C-H Yang, D. Kan,b I. Takeuchi, V. Nagarajan and J. Seidel, *Phys. Chem. Chem. Phys.* **2012**, *14*, 15953–15962.

[4] D. C. Arnold, IEEE Transactions on Ultrasonics, Ferroelectrics, and Frequency Control, 62, 1, 2015

[5] D. Kan, C.-J. Cheng, V. Nagarajan, and I. Takeuchi, *J. of Appl. Phys.* **2011**, *110*, 014106.

[6] D. Kan, L. Palova, V. Anbusathaiah, C. J. Cheng, S. Fujino, V. Nagarajan, K. M. Rabe, and I. Takeuchi, Adv. Funct. Mater. **20**, 1108 (2010).

[7] C.-J. Cheng, D. Kan, S.-H. Lim, W. R. McKenzie, P. R. Munroe, L. G. Salamanca-Riba, R. L. Withers, I. Takeuchi, and V. Nagarajan, *Phys. Rev. B* **2009**, *80*, 014109.

[8] A.Y. Borisevich, E.A. Eliseev, A.N. Morozovska, C.-J. Cheng, J.-Y. Lin, Y.H. Chu, D. Kan, I. Takeuchi, V. Nagarajan, S.V. Kalinin, *Nat. Comm.* **2012**, *3*, 775.

[9] J. Hoppler, J. Stahn, C. Niedermayer, V.K. Malik, H. Bouyanfif, A.J. Drew, M. Rössle, A. Buzdin, G. Cristiani, H-U Habermeier, B. Keimer, C. Bernhard, *Nat. Mater.* **2009**, *8 (4)*, 315-319.

[10] H Bouyanfif, M El Marssi, N Lemée, F Le Marrec, MG Karkut, B Dkhil, *Phys. Rev. B* **2005**, *71 (2)*, 020103.

[11] H. Bouyanfif, N. Lemée, M. El Marssi, F. Le Marrec, B. Dkhil, J. Chevreul, B. Fraisse, J.C. Picot, M.G. Karkut, *Phys. Rev. B* **2007**, *76 (1)*, 014124.

[12] F. De Guerville, M. El Marssi, I. P. Raevski, M. G. Karkut, and Yu. I. Yuzyuk *Phys. Rev. B* **2006**, *74*, 064107.

[13] M. El Marssi, Y. Gagou, J. Belhadi, F. De Guerville, Yu. I. Yuzyuk and I. P. Raevski, *J. Appl. Phys.* **2010**, *108*, 084104.

[14] J. Belhadi, M. El Marssi, Y. Gagou, Yu I Yuzyuk, Y. El Mendili, I. P. Raevski, H. Bouyanfif, J. Wolfman, *J. Appl. Phys.* **2014**, **116**, 034108.

[15] J. Belhadi, M. El Marssi, Y. Gagou, Yu I Yuzyuk, I. P. Raevski, *EPL (Europhysics Letters)* **2014**, *106 (1)*, 17004.

[16] J. Sinsheimer, S.J. Callori, B. Bein, Y. Benkara, J. Daley, J. Coraor, D. Su, P.W. Stephens, and M. Dawber, *Phys. Rev. Lett.* **2012**, *109*, 167601.

[17] G. Rispens, B. Ziegler, Z. Zanolli, J. Iniguez, P. Ghosez, and P. Paruch, *Phys. Rev. B* **2014**, *90*, 104106.

[18] R. Maran, S. Yasui, E. Eliseev, A. Morozovska, H. Funakubo, I. Takeuchi, and V. Nagarajan, *Adv. Electron. Mater.* **2016**, 1600170

[19] R. Maran, S. Yasui, E. Eliseev, M. Glinchuk, A. Morozovska, H. Funakubo, I. Takeuchi, V. Nagarajan, *Phys. Rev. B* **2014**, *90*, 245131.

[20] J. Bielecki, P. Svedlindh, D. T. Tibebu, S. Cai, Sten-G. Eriksson, L. Börjesson, and C. S. Knee, *Phys. Rev. B* **2012**, *86*, 184422.

[21] A. Scholl, J. Stöhr, J. Lüning, J. W. Seo, J. Fompeyrine, H. Siegwart, J.-P. Locquet, F. Nolting, S. Anders, E. E. Fullerton, M. R. Scheinfein, H. A. Padmore, *Science*, **2000**, *287 (5455)*, 1014-1016.

[22] K. Boldyreva, D. Bao, G. Le Rhun, L. Pintilie, M. Alexe, and D. Hesse, *J. of Appl. Phys.* **2007**, *102*, 044111.

[23] K. Vaideeswaran, PhD thesis, EPFL, **2015**.

[24] S. Karimi, I. M. Reaney, I. Levin and I. Sterianou, *Appl. Phys. Lett.* **2009**, *94*, 112903.

[25] M. Tanaka, R. Saito, and K. Tsuzuki, *Jpn. J. of App. Phys.* **1982**, *21*, 291.

[26] M. Kubota, K. Oka, Y. Nakamura, H. Yabuta, K. Miura, Y. Shimakawa, M. Azuma, *Jpn. J. of Appl. Phys.* **2011**, Part 1, *50*, 09ne08.

[27] D. A. Rusakov, A. M. Abakumov, K. Yamaura, A. A. Belik, G. Van Tendeloo, and E. Takayama-Muromachi, *Chem. of Mater.* **2011**, *23 (2)*, 285-292.

[28] A. Vailionis, H. Boschker, W. Siemons, E. P. Houwman, D. H. A. Blank, G. Rijnders, and G. Koster, *Phys. Rev. B* **2011**, *83*, 064101.

[29] Y. Yang, W. Ren, M. Stengel, X. H. Yan, and L. Bellaiche, *Phys. Rev. Lett.* **2012**, 109, 057602.

[30] Z. Zanolli, J. C. Wojdeł, J. Íñiguez, and P. Ghosez, *Phys. Rev. B* **2013**, 88, 060102(R)

[31] S. Prosandeev, Dawei Wang, Wei Ren, Jorge Íñiguez and L. Bellaiche, *Adv. Funct. Mat.* **2013**, *23*, 234-40.

[32] E. Bousquet, M. Dawber, N. Stucki, C. Lichtensteiger, P. Hermet, S. Gariglio, J.-M. Triscone and P. Ghosez, *Nature*, **2008**, 452, *732.*

[33] P. Hermet, M. Goffinet, J. Kreisel, and Ph. Ghosez, *Phys. Rev. B* **2007**, *75*, 220102(R).

[34] V. Goian,S. Kamba, S. Greicius, D. Nuzhnyy, S. Karimi, and I. M. Reaney, *J. of Appl. Phys.* **2011**, *110*, 074112.

[35] M. Guennou, P. Bouvier, G. S. Chen, B. Dkhil, R. Haumont, G. Garbarino, and J. Kreisel, *Phys. Rev. B* **2011**, *84*, 174107.

[36] F. Xue, L. Liang, Y. Gu, I. Takeuchi, S. V. Kalinin, and L.-Q. Chen, *Appl. Phys. Lett.*, **2015**, *106*, 012903

[37] G. Khabiri, A.S. Anokhin, A.G. Razumnaya, Y.I. Yuzyuk, I. Gueye, B. Carcan, H. Bouyanfif, J. Wolfman, C. Autret-Lambert, M. El Marssi, *Physics of the Solid State*, **2014**, *56 (12)*, 2507-2513.

[38] I.C. Infante, S. Lisenkov, B. Dupé, M. Bibes, S. Fusil, E. Jacquet, G. Geneste, S. Petit, A. Courtial, J. Juraszek, L. Bellaiche, A. Barthélémy, B. Dkhil, *Phys. Rev. Lett.* **2010**, *105*, 057601.

[39] H. Toupet, F. Le Marrec, C. Lichtensteiger, B. Dkhil, and M. G. Karkut, *Phys. Rev. B* **2010**, *81*, 140101(R).

[40] X. Martí, P. Ferrer, J. Herrero-Albillos, J. Narvaez, V. Holy, N. Barrett, M. Alexe, and G. Catalan, *Phys. Rev. Lett.* **2011**, *106*, 236101.

[41] R. Haumont, Igor A. Kornev, S. Lisenkov, L. Bellaiche, J. Kreisel, and B. Dkhil, *Phys. Rev. B* **2008**, *78*, 134108.

[42] C. Cazorla and M. Stengel, *Phys. Rev. B* **2014**, 90, 020101(R).